Measurement of the Thermal Conductivity and Heat Capacity of Freestanding Shape Memory Thin Films Using the 3ω Method

Ankur Jain[1]
e-mail: ankurjain@stanfordalumni.org

Kenneth E. Goodson

Department of Mechanical Engineering,
Stanford University,
Stanford, CA 94305

An accurate measurement of the thermophysical properties of freestanding thin films is essential for modeling and predicting thermal performance of microsystems. This paper presents a method for simultaneous measurement of in-plane thermal conductivity and heat capacity of freestanding thin films based on the thermal response to a sinusoidal electric current. An analytical model for the temperature response of a freestanding thin film to a sinusoidal heating current passing through a metal heater patterned on top of the thin film is derived. Freestanding thin-film samples of silicon nitride and nickel titanium (NiTi), a shape memory alloy, are microfabricated and characterized. The thermal conductivity of thin-film NiTi, which increases linearly between 243 K and 313 K, is 40% lower than the bulk value at room temperature. The heat capacity of NiTi also increases linearly with temperature in the low temperature phase and is nearly constant above 280 K. The measurement technique developed in this work is expected to contribute to an accurate thermal property measurement of thin-film materials. Thermophysical measurements on NiTi presented in this work are expected to aid in an accurate thermal modeling of microdevices based on the shape memory effect. [DOI: 10.1115/1.2945904]

Keywords: thermal conductivity, thin film, 3ω method, shape memory effect, thermal characterization, microfabrication, heat capacity

1 Introduction

Freestanding thin films are used in a variety of microelectromechanical systems (MEMS)–based applications such as micropumps [1], gas sensors [2], pressure sensors [3], microvalves [4], and microactuators [5]. The performance of such MEMS-based systems is often linked to thermal conduction phenomena in the device. For example, in a thin-film microheater device, the response time and maximum temperature reached are functions of the heat capacity and thermal conductivity of the thin-film material. Thermophysical properties of thin films deviate significantly from the bulk-form value due to a variety of reasons including boundary effects [6]. Apart from thickness, there is also a strong dependence on the method of deposition of the thin film [7,8] and on temperature [9,10]. *In situ* thermophysical measurement is thus essential for accurate modeling and performance prediction of thermal-based microdevices.

There are a broad variety of electrical and optical methods for the measurement of thermal properties of thin films [11,12]. Methods based on electrical heating are among the most popular and use either steady-state or transient heating. The steady-state electrical methods involve passing direct current through a metal heater and measuring the temperature rise, either by using a separate temperature sensor or by using the heater itself as a thermometer. The temperature rise may be used to determine the thermal conductivity of the material of interest using, for example, the Fourier law of heat conduction. Transient methods typically measure either the time response of the material of interest to a heating signal or the thermal response to sinusoidal heating generated by an alternating current. Apart from electrical methods, techniques based on other phenomena such as reflectance [13,14] and photoacoustics [15,16] have also been used.

The thermophysical properties of thin films deposited on a thick substrate of well-known thermal properties have been measured in a number of papers using a variety of methods [17–19]. For example, the 3ω method has been used to determine thin-film thermal conductivity by assuming the thermal resistances through the thin film and the substrate to add up in series [20]. The thermal conductivity is then determined by measuring the thermal response of a film-on-substrate system and comparing it with the thermal response expected in the absence of the thin film. However, such a measurement does not take into account the thermal contact resistance between the thin film and substrate, which is known to play a significant role in heat transfer in microstructures. In addition, the heat capacity of the thin-film material cannot be measured using this method. While there is a wide literature on thermal measurements on a thin film deposited on a substrate, only a limited number of measurements have been made on freestanding thin films [21–23].

This paper develops a variation of the 3ω method for a simultaneous measurement of in-plane thermal conductivity and heat capacity of freestanding thin films. The method is applied to silicon nitride and nickel titanium (NiTi) films of thickness near 1 μm. NiTi is a shape memory alloy that has attracted much research in the MEMS community due to its interesting mechanical properties [24,25]. The capability of shape memory alloys to recover large thermal strains has been used in actuation-based microdevices such as micropumps and microvalves. [1,5]. The work output of thin-film shape memory based actuation is superior to other comparable actuation technologies [24]. More recently, the excellent chemical resistance and biocompatibility of shape memory alloys have led to the development of exciting biomedical applications, including stents and drug delivery [26], tissue fixation [27], etc.

[1]Present address: Freescale Semiconductor, Austin, TX 78754.

Contributed by the Heat Transfer Division of ASME for publication in the JOURNAL OF HEAT TRANSFER. Manuscript received June 4, 2007; final manuscript received January 11, 2008; published online August 8, 2008. Review conducted by Yogendra Joshi.

Downloaded 18 Nov 2008 to 171.64.49.29. Redistribution subject to ASME license or copyright; see http://www.asme.org/terms/Terms_Use.cfm

NiTi is a nearly stoichiometrically equal alloy of Ni and Ti. While NiTi has been widely used in its bulk form, its application to MEMS was long hindered by difficulties in depositing thin films of NiTi with accurately controlled stoichiometric ratio of Ni and Ti [28]. This led to problems in reproducing the shape memory effect, which is extremely sensitive to the ratio of the constituent elements in the shape memory alloy. Robust techniques based on two-source sputter deposition have recently been developed for obtaining good quality thin films of NiTi [29]. This, combined with other microfabrication capabilities makes thin-film shape memory alloys very attractive for actuation related MEMS applications, including micropumps, microgrippers, etc.

While the electric and mechanical properties of shape memory alloys have been well investigated, there has been relatively lesser work in characterizing their thermophysical properties. Since the actuation of shape memory microdevices occurs by temperature modulation due to electrical heating, the thermophysical properties of the thin-film shape memory material play an important role in determining its performance characteristics. While some thermal conductivity measurements of shape memory materials have been reported [30–32], none of this work addresses the thin-film form. Thus, an investigation of thermophysical properties of thin-film shape memory alloys may lead to a better understanding of their thermomechanical behavior and the development of more accurate performance prediction tools for shape memory based microdevices.

The next section presents the derivation of the 3ω response of a freestanding thin film to a sinusoidal electric current passed through a metal heater patterned on top of it. Design and microfabrication of MEMS-based freestanding thin-film structures are described next, followed by a discussion of the experimental data and comparison with the analytical model.

2 Theory

The 3ω method [17] is a powerful tool for thermophysical property measurement and has been used extensively for a wide variety of materials including dielectrics [18,33], superlattice materials [34], complex alloys [19], etc. The 3ω method is based on the temperature-dependent electrical resistivity of metals. A thin metal line is deposited on the material of interest, and a small sinusoidal electric current is passed through it. Since the electric current is sinusoidal at frequency ω, the resultant Joule heating, and hence the temperature of the metal line, has a component that oscillates at a frequency of 2ω. The amplitude of this temperature oscillation is a function of the heating power, geometry, and thermophysical properties of the material of interest. Thus, the measurement of the 2ω temperature oscillation amplitude provides a means of determining the thermal properties of the material. This measurement is performed indirectly by measuring the 3ω voltage induced due to the electric current that oscillates at frequency ω and the temperature-dependent electrical resistance of the metal heater, which oscillates at frequency 2ω. The two quantities are related by the following equation [17,35]:

$$\Delta T_{2\omega} = 2\frac{dT}{dR}\frac{R}{V}V_{3\omega} \tag{1}$$

The 3ω method was first used for measurements on a substrate that was much thicker than the thermal penetration depth of the thermal wave produced by the sinusoidal current. In this case, a semi-infinite assumption was used to simplify and solve the governing energy equation. This method fails for freestanding thin films since the current frequency would have to be unrealistically high to still satisfy the semi-infinite assumption. The 3ω method has been modified for measuring thermal properties of thin films deposited on a substrate with well-known properties [20]. In this case, the thermal resistances through the thin film and the substrate are assumed to add up in series. Thus, the temperature oscillation amplitude with the thin film exhibits a constant frequency-independent difference from the value expected if only the substrate were present. This difference is used to determine the thermal conductivity of the thin film. This method cannot measure the heat capacity of the thin film. In addition, the boundary thermal resistance between the thin film and substrate remains unaccounted for. Some work has also been done on using numerical simulations for applying the 3ω method for freestanding thin films [36]. However, the development of an analytical method for thermal measurements remains highly desirable.

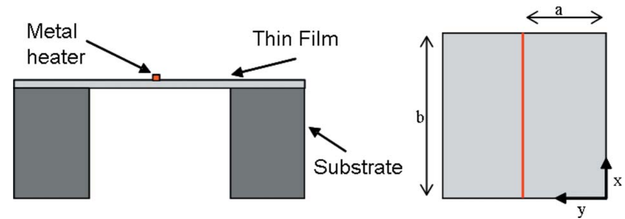

Fig. 1 Schematic showing the geometry of the freestanding thin film suspended on a substrate

Consider the geometry shown in Fig. 1. The thin-film membrane is supported all around by a substrate material. While the method outlined in this work may be used for any geometry, a rectangular membrane with dimensions $2a$ and $2b$ is considered in detail here. The thickness of the membrane is t_m. A metal heater of width w and height h is patterned in the center of the membrane. w and h are both small compared to the membrane dimensions. Thus, heat transfer within the metal may be neglected and the metal heater may be treated as a line source of heat. The metal heater is assumed to carry sinusoidal electric current of amplitude I and frequency ω. The electrical resistance of the metal heater is R. The out-of-plane thin-film thermal resistance is assumed to be small compared to the in-plane thermal resistance, so that the thin film may be treated as isothermal in the z-direction. Further simplification may be obtained by assuming convection and radiation to be negligible compared to conduction in the membrane plane. Under these assumptions, the governing energy equation may be simplified to

$$\frac{\partial^2\theta}{\partial x^2} + \frac{\partial^2\theta}{\partial y^2} = \frac{\dot{q}'''}{k} + \frac{1}{\alpha}\frac{\partial\theta}{\partial t} \tag{2}$$

where θ represents the temperature rise over the substrate temperature. Note that $\dot{q}^m$ is the volumetric heat generation rate and α is the thermal diffusivity.

In order to solve the energy equation, the membrane is divided into two equal parts separated by the metal heater. Thus the metal heater forms one of the domain boundaries, and heat generation in the metal heater may be modeled as a heat flux boundary condition. The membrane boundaries may be assumed to be isothermal due to the large thermal mass of the substrate material. Thus, the boundary conditions and initial condition for Eq. (2) may be written as

$$\theta(0,y,t) = \theta(b,y,t) = \theta(x,0,t) = 0$$

$$\frac{\partial\theta}{\partial y}^{y=a} = \frac{I^2\sin^2(\omega t)R}{2k(t_m b)} = \frac{I^2 R}{2k(t_m b)}\left(\frac{1-\cos(2\omega t)}{2}\right) \tag{3}$$

$$\theta(x,y,0) = 0$$

The governing energy equation derived here is a linear time-dependent partial differential equation (PDE) with all homogeneous boundary conditions except one. In order to solve this PDE, the solution is assumed to be the sum of a steady-state component $\theta_{ss}(x,y)$ corresponding to the steady component of Joule heating due to the sinusoidal current and a time-dependent component $\theta_{tr}(x,y,t)$ that consists of the transient and sinusoidal terms. The

Downloaded 18 Nov 2008 to 171.64.49.29. Redistribution subject to ASME license or copyright; see http://www.asme.org/terms/Terms_Use.cfm

solution for the steady-state component is easily determined using the method of separation of variables to be

$$\theta_{ss}(x,y) = \sum_{n=1}^{\infty} -\frac{I^2R(1-\cos(n\pi))}{2kt_m(n\pi)^2\cosh\left(\frac{n\pi a}{b}\right)}\sin\left(\frac{n\pi x}{b}\right)\sinh\left(\frac{n\pi y}{b}\right) \quad (4)$$

The method of integral transforms [37] is used to derive the solution for the transient component. This method involves assuming the solution of the nonhomogeneous problem to be a linear combination of the general solutions of the corresponding homogeneous problems and deriving ODEs for the time-dependent coefficients in the linear combination. The solution for the transient temperature response is found out to be

$$\theta_{tr}(x,y,t) = \sum_{m=1}^{\infty}\sum_{n=1}^{\infty} C_{m,n}(t)\sin\left(\frac{n\pi x}{b}\right)\sin\left(\frac{(m+1/2)\pi y}{a}\right) \quad (5)$$

where

$$C_{m,n}(t) = \frac{4\omega^2}{\gamma_{m,n}^2+4\omega^2}\frac{\zeta_{m,n}}{2\gamma_{m,n}}e^{-\gamma_{m,n}t} + \frac{\zeta_{m,n}}{2\sqrt{\gamma_{m,n}^2+4\omega^2}}\sin(2\omega t+\varphi_{m,n}) \quad (6)$$

The phase angle $\varphi_{m,n}$ may be expressed in terms of the input parameters as follows:

$$\varphi_{m,n} = \tan^{-1}\left(\frac{\gamma_{m,n}}{2\omega}\right) \quad (7)$$

Note that in Eqs. (6) and (7) above,

$$\zeta_{m,n} = (-1)^{m+1}(1-(-1)^n)\frac{4\alpha}{n\pi a}\frac{I^2R}{2kt_m b}$$
$$\gamma_{m,n} = \alpha\pi^2\left[\left(\frac{m+1/2}{a}\right)^2 + \left(\frac{n}{b}\right)^2\right] \quad (8)$$

Equations (4) and (5) represent the solution of the energy equation that governs the temperature profile on the thin-film membrane. The steady-state component of the temperature solution varies linearly with the input power, with the slope being related to the thermal conductivity of the thin film. The sinusoidal component oscillates at a frequency that is twice that of the heating current. In order to extract measurable quantities from this thermal model, the steady-state and sinusoidal temperature components are averaged along the heater by integration to yield the following average quantities for the metal heater:

$$\bar{\theta}_{av} = \sum_{n=1}^{\infty}\frac{I^2R}{2kt_m(n\pi)^3}(1-\cos(n\pi))^2\tanh\left(\frac{n\pi a}{b}\right)$$
$$\bar{\theta}_{2\omega} = \sum_{n=1}^{\infty}\sum_{m=1}^{\infty} -\frac{\zeta_{m,n}}{2\sqrt{\gamma_{m,n}^2+4\omega^2}}\frac{\sin((m+1/2)\pi)(1-\cos(n\pi))}{n\pi} \quad (9)$$

While $\bar{\theta}_{av}$ represents the average heater temperature rise due to Joule heating, $\bar{\theta}_{2\omega}$ represents the amplitude of the temperature oscillation at 2ω frequency due to the sinusoidal nature of heating. Measurement of these quantities provides two equations from which two thermophysical properties, namely, thermal conductivity and thermal diffusivity (or heat capacity), may be determined. Note that only thermal conductivity appears in the equation for $\bar{\theta}_{av}$. It is relatively easier to measure $\bar{\theta}_{av}$ and $\bar{\theta}_{2\omega}$ indirectly by measuring the related voltage harmonics. The relationship between the temperature quantities and voltage harmonics is as follows:

$$V_{\omega} = IR + I\frac{dR}{dT}\bar{\theta}_{av}$$
$$V_{3\omega} = 2I\frac{dR}{dT}\bar{\theta}_{2\omega} \quad (10)$$

Note that from Eq. (9),

$$\bar{\theta}_{2\omega}\to 0 \quad \text{as } \omega\to\infty, \qquad \frac{d\bar{\theta}_{2\omega}}{d\omega}\to 0 \quad \text{as } \omega\to 0 \quad (11)$$

i.e., at large frequencies, the temperature oscillation becomes too small to be measured accurately, while at the low frequency end, it is a weak function of frequency. The temperature oscillation is most sensitive to frequency in a specific frequency window where ω is comparable to γ. Physically, the high frequency behavior is explained by the fact that at large frequencies, the thermal penetration depth becomes comparable to the membrane thickness, as a result of which the boundary condition at the other side of the thin film begins to play an important role in the heat transfer problem. On the other hand, at low frequencies, the thin film has sufficient time to equilibrate, and thus the sinusoidal effect of the heating current is lost, resulting in the loss of sensitivity of the temperature oscillation to frequency.

The next section discusses the design and microfabrication of freestanding thin-film structures using MEMS technology. Thermophysical measurements using the analytical model derived in this section are described next.

3 Microfabrication and Experimental Setup

3.1 Design and Microfabrication. Freestanding thin-film structures based on MEMS technology are designed and microfabricated. Two thin-film materials are investigated—silicon nitride and NiTi. Some of the important design considerations for the thin-film structures include the material and film thickness, and the dimensions and material of the metal features. Freestanding thin films of materials such as silicon oxide tend to crumple and often break due to the high compressive stress in the oxide films. On the other hand, silicon nitride films do not show this behavior due to the tensile stress in these films. However, if the tensile stress in the films is too high, they may be prone to cracking. It is well known that the residual stress in deposited films may be controlled by changing the chemical composition of the film.

The metal heaters patterned on top of the thin film are designed to be 10 μm wide and 0.1 μm thick. These dimensions ensure high electrical resistance and reasonably low current density during operation. The film is chosen to be around 1.0 μm thick in all experiments in order to have sufficient mechanical robustness when released from the substrate. While NiTi is inherently compressive in nature, the process conditions for silicon nitride are chosen in order to result in a film with a small amount of tensile stress.

Microfabrication is carried out at the Stanford Nanofabrication Facility (SNF). 4 in., 300 μm thick, double side polished Si wafers are used. A thin layer of thermal oxide is first grown on the wafers in order to electrically passivate the thin film of interest from the silicon substrate. This step is omitted when the thin-film material is an insulator. This is followed by deposition of the thin film of interest. The silicon nitride film is deposited in a low pressure chemical vapor deposition (LPCVD) furnace at 850°C. A high ratio of dichlorosilane to ammonia of 14:1 ensures a silicon-rich film with low residual tensile stress. The NiTi film is sputter deposited at less than 100°C in an argon atmosphere at a base pressure of 10^{-7} Torr. Following the film deposition, the wafers are annealed at 500°C in vacuum for a few minutes and allowed to cool down to room temperature. NiTi deposition is carried out by the TiNi Alloy Company, San Leandro, CA. Phase transformation temperature of the sputtered NiTi films is around

Downloaded 18 Nov 2008 to 171.64.49.29. Redistribution subject to ASME license or copyright; see http://www.asme.org/terms/Terms_Use.cfm

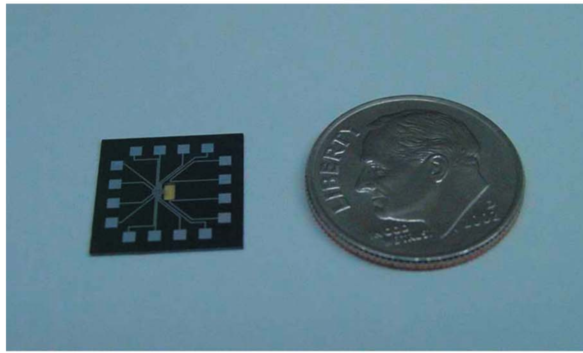

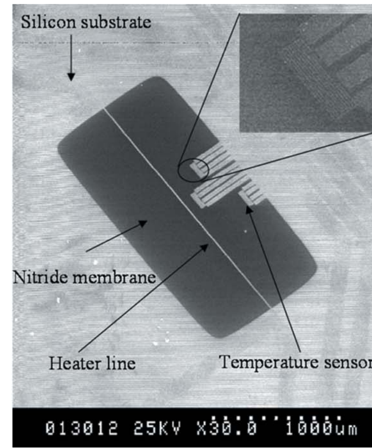

Fig. 2 A picture and SEM showing the silicon nitride freestanding thin-film microdevice

0°C. Following sputtering, the NiTi film is passivated by a 0.4 μm low temperature oxide (LTO) film deposited in a LPCVD furnace at 400°C. 0.1 μm aluminum is then sputtered on the wafers. Metal features are defined using photolithography and metal etch in a plasma etcher. Front-to-backside photolithography is then performed in order to define features to be etched on the wafer backside. Following the attachment of a backing wafer using photoresist, the wafers are etched from the backside in a deep reactive ion etcher. Due to nonuniform etching across the wafer, the etching is stopped when about 10–20 μm silicon is left, and the wafers are diced. Individual devices are then separately etched to completion. This minimizes overetching of the thin film of interest. Photoresist is washed off in acetone, and individual devices are packaged in a ceramic chip carrier. Electrical contact pads are wire bonded. Figure 2 shows a picture and scanning electron micrograph (SEM) of a silicon nitride thin-film structure microfabricated in this manner. Note that the film is stretched out due to the residual tensile stress in silicon nitride. On the other hand, NiTi is compressive in nature, and thus the NiTi thin films are wavy in nature, as shown in Fig. 3.

3.2 Experimental Setup. Figure 4 shows a schematic of the experimental setup used for thermophysical characterization of freestanding thin films. The setup consists of a vacuum chamber with a temperature-controlled platform. A proportional-integral-derivative (PID) controller maintains the desired platform temperature using liquid nitrogen and a Joule heater. The ceramic package carrying the MEMS device is attached to the platform. Wires soldered to gold pads on the ceramic package are used to electrically probe the MEMS device. The chamber is connected to a vacuum pump capable of delivering a pressure of 10 mTorr. All experiments are performed at 10 mTorr or less in order to rule out convective effects. Radiative losses are also negligible due to the small temperature rise in the samples. An SRS 830 lock-in amplifier is used for supplying sinusoidal electric current and for measuring voltage harmonics V_{ω} and $V_{3\omega}$ generated across the metal heater. An HP 3458A multimeter is used for current measurement. Since the third harmonic of voltage is much smaller than the first harmonic, an accurate measurement of the former requires the arrangement of the metal heater as one of the arms of a Wheatstone bridge. The bridge is balanced using a variable resistor arm. The third harmonic of voltage is then easily measured across the balanced bridge, while the first harmonic of voltage is directly measured across the metal heater.

4 Results and Discussion

As a first step, the electrical resistance of the metal heater is measured as a function of temperature. The test current is chosen

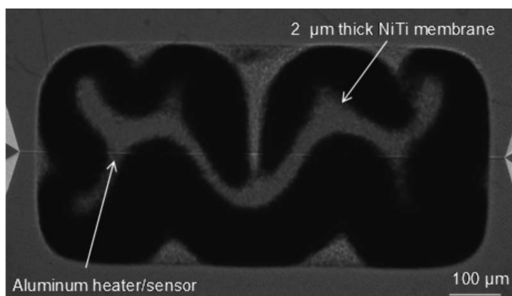

Fig. 3 An image of the freestanding NiTi thin film. Note the ridgy membrane surface due to the compressive residual stress in the film.

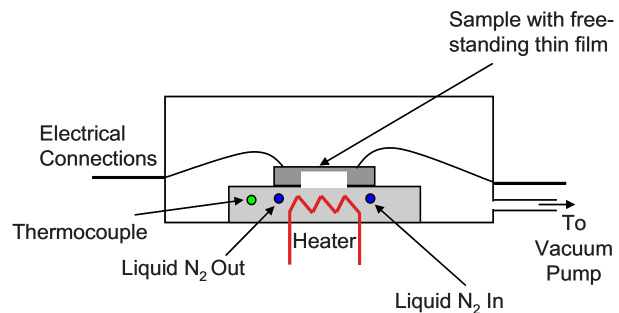

Fig. 4 A schematic of the experimental setup used for temperature-dependent thermophysical measurements on freestanding thin films

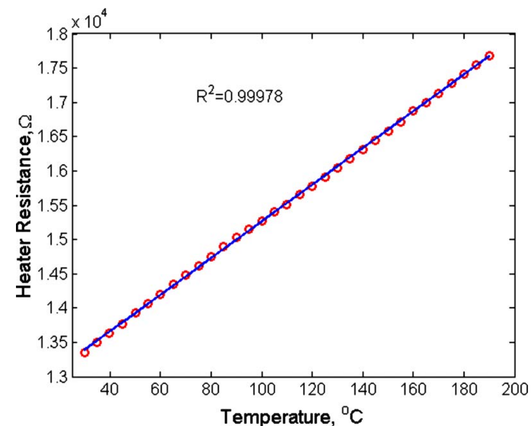

Fig. 5 Plot of the heater electrical resistance as a function of temperature. A linear temperature dependence is observed as expected.

Downloaded 18 Nov 2008 to 171.64.49.29. Redistribution subject to ASME license or copyright; see http://www.asme.org/terms/Terms_Use.cfm

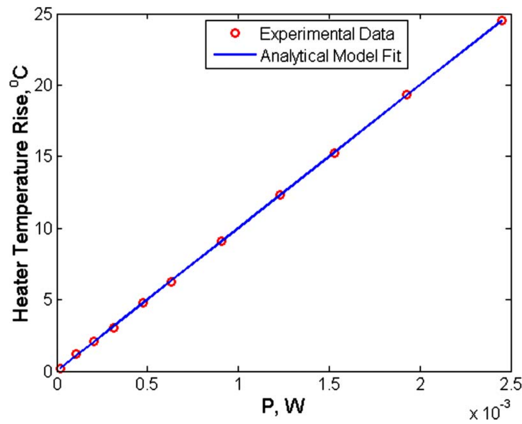

Fig. 6 Heater temperature rise as a function of the input heating power. As expected, the temperature rise depends linearly on the heating power. There is a good agreement between the experimental data and the analytical model. Thermal conductivity of the freestanding thin film may be determined from the slope of the plot.

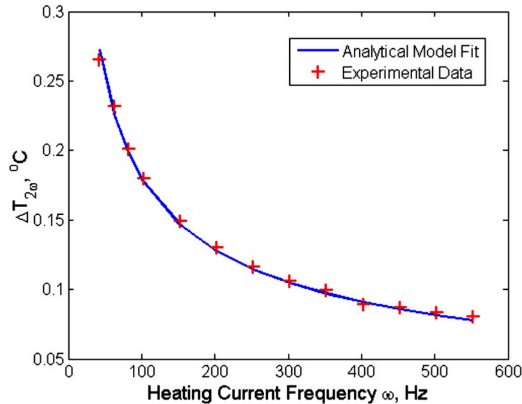

Fig. 7 2ω temperature oscillation amplitude as a function of the frequency of heating current. Experimental data agree well with the analytical model. Using the thermal conductivity value determined from the temperature rise data, least-squares fitting of experimental data with Eq. (9) yields the value of thermal diffusivity of the freestanding thin film.

to be small enough to not cause significant self-heating. As shown in Fig. 5, the electrical resistance is found to be a linear function of temperature, with a temperature coefficient of 0.0022 K^{-1}. Next, the heater temperature rise is measured as a function of heating power. Figure 6 shows a plot of the average temperature rise as a function of the heating power. As expected, the average temperature rise has a linear dependence on the heating power. There is a good agreement between experimental data and the analytical model presented in Sec. 2. Thermal conductivity of the freestanding thin film may be determined from the slope of the least-squares fit of the analytical model to the experimental data. Once the thermal conductivity has been determined, the amplitude of 2ω temperature oscillation is measured and plotted as a function of the frequency of the electric current. As shown in Fig. 7, there is a good agreement between the experimental data and the analytical model represented by Eq. (9). The temperature oscillation is most sensitive to frequency in a window of roughly 40–1000 Hz. With the thermal conductivity already determined using the average heater temperature rise, least-squares fitting of experimental data for the 2ω temperature oscillation is used to determine the thermal diffusivity of the thin film. Heat capacity of the film can also be determined by combining the two measurements. Using the temperature-controlled platform, the measurements are repeated over a large temperature range, thus yielding temperature-dependent data for thermal conductivity and heat capacity of the freestanding thin film. 10 minutes are allowed before each measurement in order for the temperature to become steady. Figure 8 shows a plot of the thermal conductivity and heat capacity of a 1.5 μm silicon nitride film between $-200°C$ and $200°C$. Both thermal conductivity and heat capacity increase with temperature, with the temperature dependence of thermal conductivity being stronger. This measured temperature data are consistent with previous measurements [18,38].

The experimental procedure is also used for thermophysical characterization of thin-film NiTi. Figure 9 shows the thermal conductivity and heat capacity of 1.7 μm thick NiTi film over a temperature range of $-40°C$ and $40°C$. Thermal conductivity of NiTi is observed to increase linearly as a function of temperature. On the other hand, heat capacity increases with temperature from $-30°C$ to about $0°C$, following which it remains constant. This may be related to the phase change that occurs in the NiTi film at around $0°C$. While the heat capacity of one of the NiTi phases increases with temperature, the other phase has a much weaker temperature dependence of the heat capacity. Table 1 summarizes the room-temperature measurements of thermal conductivity and heat capacity of thin-film silicon nitride and NiTi.

Thermophysical measurements on thin-film shape memory alloys have not been reported in the past. The thermal conductivity

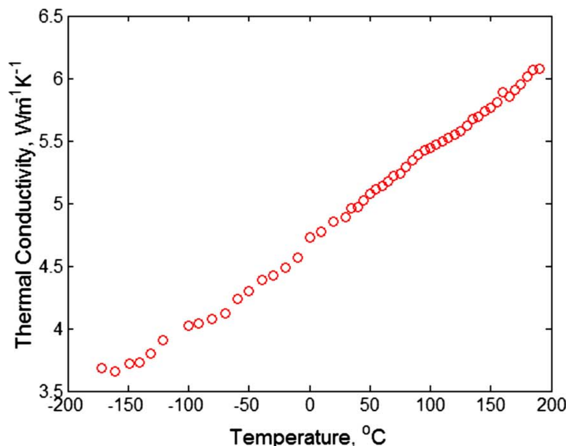

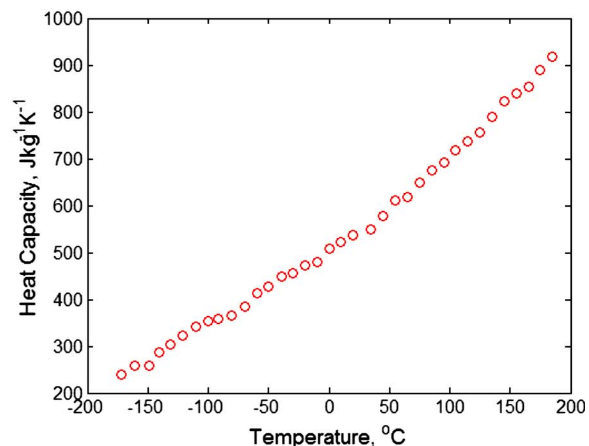

Fig. 8 Temperature dependence of thermal conductivity and heat capacity for 1.5 μm silicon nitride film

Downloaded 18 Nov 2008 to 171.64.49.29. Redistribution subject to ASME license or copyright; see http://www.asme.org/terms/Terms_Use.cfm

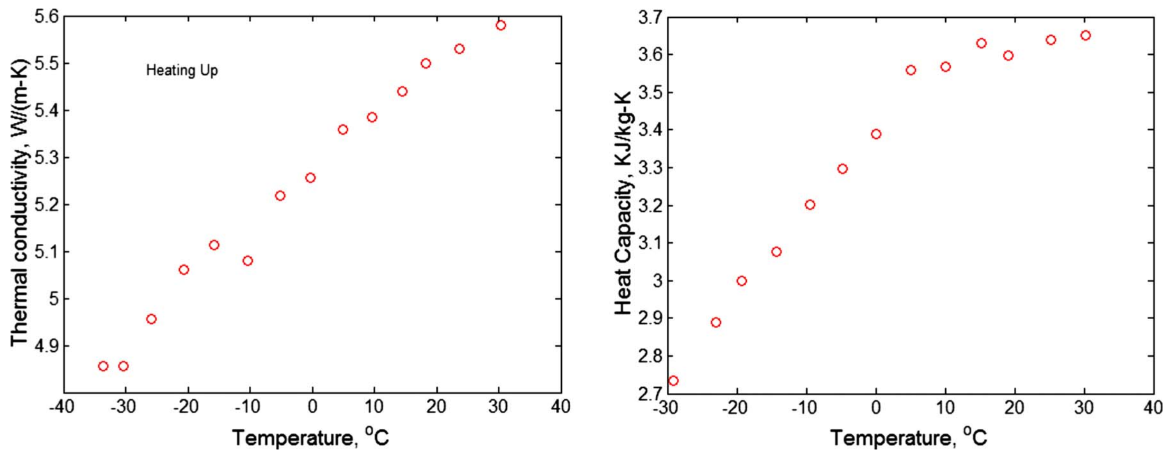

Fig. 9 Temperature dependence of thermal conductivity and heat capacity for 1.7 μm NiTi film. Note that the phase transformation temperature of NiTi is around 0°C.

Table 1 Summary of the room-temperature thermophysical thin-film data measured in this work

	Thermal conductivity, $W\ m^{-1}\ K^{-1}$	Heat capacity, $J\ kg^{-1}\ K^{-1}$
Silicon nitride	4.9 ± 0.7	523.2 ± 78.5
NiTi	5.5 ± 0.8	3612.3 ± 581.3

of NiTi measured in this work is about 40% smaller than the well-known bulk value [30]. The thermal conductivity reduction underlines the importance of measuring thin-film properties *in situ* instead of using previously measured bulk-form values when developing analytical or numerical models for predicting the performance of shape memory alloy based MEMS devices. The mechanism behind this significant reduction in thermal conductivity is currently under investigation. It is possible that this deviation from bulk value is due to a different stoichiometric composition compared to the previous work. Shape memory material properties are known to be extremely sensitive to composition. If the bulk samples used by Goff [30] were crystalline, it is possible that defects in the thin-film form, augmented by an offset in the stoichiometric ratio, may be playing a role in the thermal conductivity reduction.

Uncertainty in the film thickness measurement is the largest source of uncertainty in the absolute measured value of thermal conductivity and heat capacity. Film thickness is measured using a Nanospec system based on noncontact spectroreflectometry. The expected error in film thickness measurements using the Nanospec is around 10%. In addition, error analysis shows that a higher electric current results in a lower uncertainty in the measured value of thermal conductivity and heat capacity. However, a higher electric current also leads to higher self-heating, which causes the averaging out of each measurement over a larger temperature range. A tradeoff between these conflicting parameters is reached by using a maximum electric current of around 0.5 mA and 6 mA for the silicon nitride and NiTi measurements, respectively, wherein the uncertainty in thermal conductivity and heat capacity measurements is around 12–15% and the maximum temperature rise in the thin film is limited to around 2°C.

5 Conclusion

The availability of accurate thermophysical data for thin-film materials plays an important role in the development of modeling tools for microsystems. The present work extends the 3ω method to freestanding thin films and develops a technique for measuring both thermal conductivity and heat capacity simultaneously. The method presented here offers several advantages over other possible methods for measuring thermal properties of freestanding thin films. The measured value of the thermal conductivity of thin-film NiTi is significantly smaller than the bulk-form value, which reinforces the need for direct thin-film measurements instead of using bulk values when developing thermal models for microsystems. The thermophysical measurements on thin-film NiTi presented here are likely to throw new light on a promising material for MEMS.

Acknowledgment

The authors would like to acknowledge financial support from the Stanford Graduate Fellowship Program (SGF), the Semiconductor Research Corporation (SRC) and a NSF NIRT Award. Microfabrication work presented in this paper was performed at the Stanford Nanofabrication Facility (SNF). Useful discussions with Kevin Ness and Xuejiao Hu are gratefully acknowledged.

Nomenclature

a = membrane width
b = membrane breadth
h = heater height
I = electric current
k = thermal conductivity
R = electrical resistance
t = time
t_m = membrane thickness
T = temperature
V = voltage
w = heater width
α = thermal diffusivity
φ = phase change
θ = temperature rise
ω = frequency

Subscripts

av = average
ss = steady state
tr = transient

References

[1] Benard, W. L., Kahn, H., Heuer, A. H., and Huff, M., 1998, "Thin-Film Shape Memory Alloy Actuated Micropumps," J. Microelectromech. Syst., **7**, pp. 245–251.

[2] Sberveglieri, G., Hellmich, W., and Müller, G., 1997, "Silicon Hotplates for Metal Oxide Gas Sensor Elements," Microsyst. Technol., **3**, pp. 183–190.

[3] Eaton, W. P., and Smith, J. H., 1997, "Micromachined Pressure Sensors: Re-

Downloaded 18 Nov 2008 to 171.64.49.29. Redistribution subject to ASME license or copyright; see http://www.asme.org/terms/Terms_Use.cfm

view and Recent Developments," Smart Mater. Struct., **6**, pp. 530–539.
[4] Kohl, M., Dittmann, D., Quandt, E., Winzek, B., Miyazaki, S., and Allen, D. M., 1999, "Shape Memory Microvalves Based on Thin Films or Rolled Sheets," Mater. Sci. Eng., A, **273–275**, pp. 784–788.
[5] Krulevitch, P., Lee, A. P., Ramsey, P. B., Trevino, J. C., Hamilton, J., and Northrup, M., 1996, "Thin Film Shape-Memory Alloy Micro-Actuators," J. Microelectromech. Syst., **5**(4), pp. 270–282.
[6] Cahill, D. G., Ford, W. K., Goodson, K. E., Mahan, G. D., Majumdar, A., Maris, H. J., Merlin, R., and Phillpot, S. R., 2003, "Nanoscale Thermal Transport," J. Appl. Phys., **93**(2), pp. 793–818.
[7] McConnell, A. D., Uma, S., and Goodson, K. E., 2001, "Thermal Conductivity of Doped Polysilicon Layers," J. Microelectromech. Syst., **10**(3), pp. 360–369.
[8] Ju, Y. S., and Goodson, K. E., 1999, "Process-Dependent Thermal Transport Properties of Silicon Dioxide Films Deposited Using Low-Pressure Chemical Vapor Deposition," J. Appl. Phys., **85**, pp. 7130–7134.
[9] Goodson, K. E., Flik, M. I., Su, L. T., and Antoniadis, D. A., 1993, "Annealing-Temperature Dependence of the Thermal Conductivity of LPCVD Silicon-Dioxide Layers," IEEE Electron Device Lett., **14**(10), pp. 490–492.
[10] Asheghi, M., Touzelbaev, M. N., Goodson, K. E., Leung, Y. K., and Wong, S. S., 1998, "Temperature-Dependent Thermal Conductivity of Single-Crystal Silicon Layers in SOI Substrates," ASME J. Heat Transfer, **120**(1), pp. 30–36.
[11] Cahill, D. G., Goodson, K. E., and Majumdar, A., 2002, "Thermometry and Thermal Transport in Micro/Nanoscale Solid-State Devices and Structures," ASME J. Heat Transfer, **124**(2), pp. 223–241.
[12] Goodson, K. E., and Ju, Y. S., 1999, "Heat Conduction in Novel Electronic Films," Annu. Rev. Mater. Sci., **29**, pp. 261–293.
[13] Paddock, C. A., and Eesley, G. L., 1986, "Transient Thermoreflectance From Thin Metal Films," J. Appl. Phys., **60**, pp. 285–290.
[14] Chu, D. C., Touzelbaev, M., Goodson, K. E., Babin, S., and Pease, R. F. W., 2001, "Thermal Conductivity Measurements of Thin-Film Resist," J. Vac. Sci. Technol. B, **19**(6), pp. 2874–2877.
[15] Govorkov, S., Ruderman, W., Horn, M. W., Goodman, R. B., and Rothschild, M., 1997, "A New Method for Measuring Thermal Conductivity of Thin Films," Rev. Sci. Instrum., **68**(10), pp. 3828–3834.
[16] Rajan, M. A. J., Vivekanandam, T. S., Ramakrishnan, S. K., Ramachandran, K., and Umapathy, S., 2004, "Heat Transfer in Poly(Methyl Acrylate) by Photoacoustic Measurements," J. Appl. Polym. Sci., **93**(3), pp. 1071–1076.
[17] Cahill, D. G., 1990, "Thermal Conductivity Measurement From 30 K to 750 K—the 3-Omega Method," Rev. Sci. Instrum., **61**, pp. 802–808.
[18] Lee, S.-M., Cahill, D. G., and Allen, T. H., 1995, "Thermal Conductivity of Sputtered Oxide Films," Phys. Rev. B, **52**, pp. 253–257.
[19] Liu, W., and Balandin, A. A., 2005, "Thermal Conduction in $Al_xGa_{1-x}N$ Alloys and Thin Films," J. Appl. Phys., **97**, p. 073710.
[20] Cahill, D. G., Katiyar, M., and Abelson, J. R., 1994, "Thermal Conductivity of a-Si:H Thin Films," Phys. Rev. B, **50**, pp. 6077–6081.
[21] Kurabayashi, K., Asheghi, M., Touzelbaev, M., and Goodson, K. E., 1999, "Measurement of the Thermal Conductivity Anisotropy in Polyimide Films," J. Microelectromech. Syst., **8**(2), pp. 180–191.
[22] Völkein, F., and Baltes, H., 1992, "A Microstructure for Measurement of Thermal Conductivity of Polysilicon Thin Films," J. Microelectromech. Syst., **1**, pp. 193–196.
[23] Rogers, J. A., Yang, Y., and Nelson, A., 1994, "Elastic Modulus and Inplane Thermal Diffusivity Measurements in Thin Polyimide Films Using Symmetry-Selective Real-Time Impulsive Stimulated Thermal Scattering," Appl. Phys. A: Solids Surf., **58**, pp. 523–534.
[24] Fu, Y., Du, H., Huang, W., Zhang, S., and Hu, M., 2004, "TiNi-Based Thin Films in MEMS Applications: A Review," Sens. Actuators, A, **A112**(2–3), pp. 395–408.
[25] Kahn, H., Huff, M. A., and Heuer, A. H., 1998, "The TiNi Shape-Memory Alloy and Its Applications for MEMS," J. Micromech. Microeng., **8**, pp. 213–221.
[26] Reynaerts, D., Peirs, J., and Van Brussel, H., 1997, "An Implantable Drug-Delivery System Based on Shape-Memory Alloy Micro-Actuation," Sens. Actuators, A, **A61**, pp. 455–462.
[27] Xu, W., Frank, T. G., Stockham, G., and Cuschieri, A., 1999, "Shape Memory Alloy Fixator System for Suturing Tissue in Minimal Access Surgery," Ann. Biomed. Eng., **27**, pp. 663–669.
[28] Wolf, R. H., and Heuer, A. H., 1995, "TiNi (Shape Memory) Films on Silicon for MEMS Applications," J. Microelectromech. Syst., **4**, pp. 206–212.
[29] Shih, C. L., Lai, B. K., Kahn, H., Philips, S. M., and Heuer, A. H., 2001, "A Robust Co-Sputtering Fabrication Procedure for TiNi Shape-Memory Alloys for MEMS," J. Microelectromech. Syst., **10**, pp. 69–79.
[30] Goff, J. F., 1964, "Thermal Conductivity, Thermoelectric Power, and the Electrical Resistivity of Stoichiometric TiNi in the 3 to 300 K Temperature Range," J. Appl. Phys., **35**, pp. 2919–2927.
[31] Terada, Y., Ohkubo, K., Nakagawa, K., Mohri, T., and Suzuki, T., 1995, "Thermal Conductivity of B2-Type Aluminides and Titanides," Intermetallics, **3**, pp. 347–355.
[32] Faulkner, M. G., Amalraj, J. J., and Bhattacharyya, A., 2000, "Experimental Determination of Thermal and Electrical Properties of Ni-Ti Shape Memory Wires," Smart Mater. Struct., **9**, pp. 643–639.
[33] Ju, Y. S., Kurabayashi, K., and Goodson, K. E., 1999, "Thermal Characterization of Anisotropic Thin Dielectric Films Using Harmonic Joule Heating," Thin Solid Films, **339**, pp. 160–164.
[34] Yang, B., Liu, W. L., Liu, J. L., Wang, K. L., and Chen, G., 2002, "Measurements of Anisotropic Thermoelectric Properties in Superlattices," Appl. Phys. Lett., **81**(19), pp. 3588–3590.
[35] Cahill, D. G., 2002, "Errata—Thermal Conductivity Measurement From 30 K to 750 K—The 3-Omega Method," Rev. Sci. Instrum., **73**(10), pp. 3701–3701.
[36] Jacquot, A., Lenoir, B., Dauscher, A., Stolzer, M., and Meusel, J., 2002, "Numerical Simulation of the 3ω Method for Measuring the Thermal Conductivity," J. Appl. Phys., **91**(7), pp. 4733–4738.
[37] Myers, G. E., 1998, *Analytical Methods in Conduction Heat Transfer*, 2nd ed., AMCHT, Madison, WI.
[38] Mastrangelo, C. H., Tai, Y.-C., and Muller, R. S., 1990, "Thermophysical Properties of Low-Residual Stress, Silicon-Rich, LPCVD Silicon Nitride Films," Sens. Actuators, A, **A21–A23**, pp. 856–860.

Downloaded 18 Nov 2008 to 171.64.49.29. Redistribution subject to ASME license or copyright; see http://www.asme.org/terms/Terms_Use.cfm